INL/EXT-17-43685-Revision-0

Quarterly Management Document – FY17, 4th Quarter, Physics-based Creep Simulations of Thick Section Welds in High Temperature and Pressure Applications

Thomas Lillo

October 2017

The INL is a U.S. Department of Energy National Laboratory
operated by Battelle Energy Alliance

INL/EXT-17-43685-Revision-0

Quarterly Management Document – FY17, 4th Quarter, Physics-based Creep Simulations of Thick Section Welds in High Temperature and Pressure Applications

Thomas Lillo

October 2017

Idaho National Laboratory
Idaho Falls, Idaho 83415

http://www.inl.gov

Prepared for the
U.S. Department of Energy
Office of Fossil Energy
Under DOE Idaho Operations Office
Contract DE-AC07-05ID14517

Quarterly Management Document – FY17, 4th Quarter, Physics-based Creep Simulations of Thick Section Welds in High Temperature and Pressure Applications

Document # INL/EXT-17-43685

WBS Element	Project Title	Contract Number	Contract Start	Contract End
C.B.10.02.02.40	Physics-based Creep Simulations of Thick Section Welds in High Temperature and Pressure Applications	FEAA90	10/01/16	09/30/2017

Performer Name and Address	Principal Investigator(s)
Thomas Lillo Idaho National Laboratory P.O. Box 1625 Idaho Falls, ID 83415	Thomas Lillo

BUDGET AND COST REPORT

Prior Year Funds ($K)	56
Total Current Year Commitment ($K)	361
Projected Current Year Costs ($K)	317

	O	N	D	J	F	M	A	M	J	J	A	S
Monthly Planned Costs	15	15	15	23	25	33	28	28	30	35	35	35
Actual Monthly Costs	14.4	7.9	14.8	13.0	14.6	47.2	32.8	33.0	38.5	20.5	30.1	14.2
Monthly Variance	0.6	7.1	0.2	10.0	10.4	-14.2	-4.8	-5	-8.5	14.5	4.9	20.8
Total costs – planned	15	30	45	68	93	126	154	182	212	247	282	317
Total costs - actual	14.4	22.3	37.1	50.1	64.7	111.9	144.7	177.7	216.2	236.7	266.8	281.0

MILESTONE REPORT

Milestone Designation	Milestone Description	Due Date	Revised Due Date	Completion Date
A	Evaluate current MOOSE capabilities	09/30/2015		09/30/2015
B	Complete Alloy 617 weld characterization	10/30/2015		11/18/2015
C	Receipt of Alloy 740H plates	10/30/2015		11/05/2015
D	Complete welds in Alloy 740H	11/16/2015	7/31/2016	7/31/2016

E	Characterize Alloy 740H welds	02/01/2016	09/30/2016	9/02/2016
F	Creep model development – Stage 1	09/30/2016		9/30/2016
G	Creep Model Development – Stage 2	8/29/2017	12/30/2017	
H	Calibration of Secondary creep	9/30/2017	02/28/2018	
I	Stress Drop Tests	2/01/2017	3/30/2018	
J	Characterization of creep failure mechanisms	4/01/2017	02/01/2018	

TECHNICAL HIGHLIGHTS

Milestone G, "Creep Model Development – Stage 2"

1. Generation of synthetic microstructures of base and weld materials

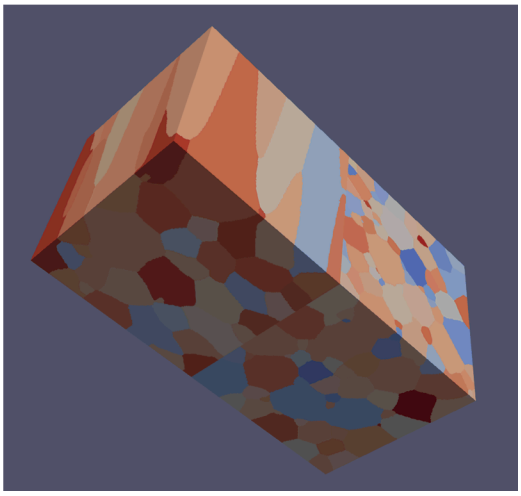

Figure 1. Microstructure generation with DREAM.3D for both base (bottom) and weld (top).

DREAM.3D [1] software can be utilized to generate synthetic microstructures using experimentally characterized EBSD data. Grain size, distribution and orientation collected from microstructure observations provide inputs for DREAM.3D to generate statically equivalent polycrystalline structures. In Figure 1, the equal-axed grains in the base metal and the elongated grains in the weld are shown next to each other. These two synthetic microstructures seem to be realistic individually, however, there is no continuously transition from one microstructure to the other one. This would become problematic for the finite element modeling. Since DREAM.3D does not have the capability to automatically stitch the two microstructures together, much effort has been made to handle merging the two microstructures through additional procedure.

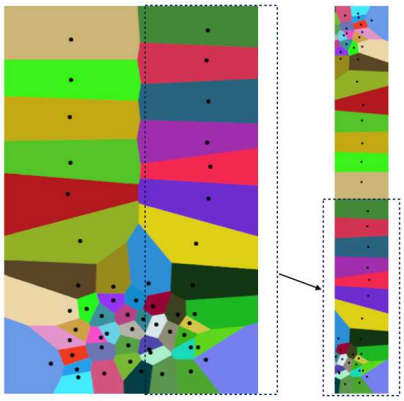

Figure 2. Continuous microstructure generated from Voronoi tessellation. Sectioning avoids the unrealistic portion of microstructure from the middle region.

The Voro++ software [2] can be used to carry out three-dimensional computations of the Voronoi tessellation based on the grain centroids coordinates taken from DREAM.3D. This allows us to generate a continuous microstructure consist of both the base and weld material from a single tessellation. The centroids output by Dream.3D correspond to the features' centers of mass and therefore take into account the edges of the volume produced. To remove the effect by the edges of the volume, only the centroids of the grains that do not touch the edge surface is used in Voronoi tessellation.

In general, this method gives a good representation of the microstructure with the exception of the unrealistic portion in the middle region shown in Figure 2. This area is unavoidable when using the Voronoi tessellation, because in order for the weld grains to be elongated in the direction that they are, centroids need to be set up at both the far left and the far right sides of the volume. This results in the weld grains from either side all meeting in the middle, which is not realistic. To mitigate this issue, the microstructure is further sectioned in order to remove the unrealistic features. The two separate sides could be stacked to create a cross-weld specimen as shown on the right of Figure 2.

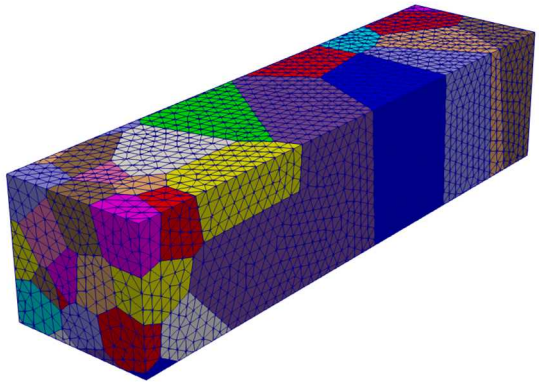

Figure 3. An example of finite element mesh generated by Cubit. It consists of base metal materials (left) and the weld materials (right).

At last, a meshing script will then utilize the outputs from Voro++ and generate a finite element mesh of the microstructure using Cubit [3], see Figure 3. The generated finite element mesh is used in the crystal plasticity finite element modeling.

Overall, this discretization work flow (DREAM3D → Voro++ → Cubit) will be used to generate synthetic microstructure of Alloy 617 and 740H welds based on EBSD.

2. Further calibration of Alloy 617 for glide and climb model

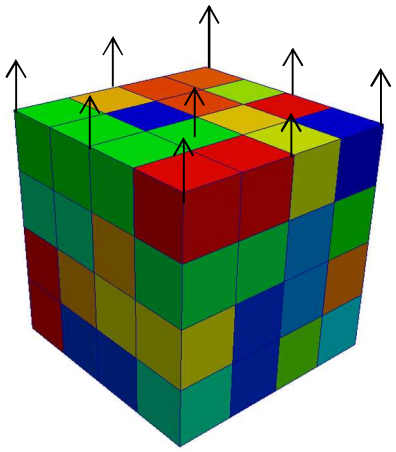

Figure 5. A cube of size 200 x 200 x 200 μm^3 with 64 grains is used. The pressure or a constant strain rate is applied on the top surface and the symmetric boundary conditions are applied on the remaining surfaces.

During a few past months, some preliminary calibration work has been done for the glide and climb model for Alloy 617. In order to make the model be able to predict the creep behavior for a wide range of temperature and pressure, further calibration is needed to identify the key parameters, which affect the creep strain.

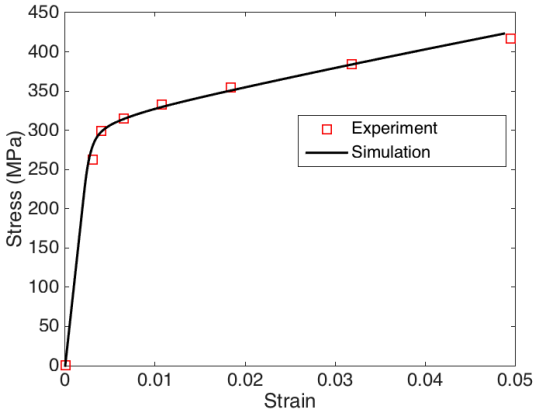

Figure 6. Strain-stress curve at room temperature for constant strain rate loading.

The experimental data for polycrystalline, equiaxed Alloy 617 alloy, provided in Wright et al [4], is used to calibrate the model parameters. We first calibrate the glide parameters using the stress-strain response of the uniaxial constant strain rate experiment at room temperature. Since the equilibrium vacancy concentration and diffusivity are extremely low at room temperature, plastic deformation is dominated by dislocation glide only. For the calibration, as shown in Figure 5, a microstructure of size 200 x 200 x 200 μm^3 with 64 cubic grains is considered and random Euler angles are assigned to each grain. The strain rate of 10^{-3} is applied. A comparison of the stress-strain curve is shown in Figure 6 and the calibrated parameters are shown in Table 1. We further investigate the effect of temperature on the yield stress and strain hardening behavior. For this case, we consider only the glide model and the effect of the temperature on the glide model comes from temperature term in the glide rate equation. Higher temperature makes the dislocation glide easier and thus lower the yield strength. The comparison of the yield strength between the simulation and experiment (Special Metals [5]) is shown in Figure 7. A good agreement can be observed, except in the temperature range of approximately 600-800ºC. In this temperature range, γ' particles are precipitating out in significant quantities which effect the resulting yield strength. Below about 600ºC, the precipitation and growth kinetics are sufficiently slow to prevent significant precipitation of γ'. Above about 750ºC, the stability of the γ' phase decreases and also the kinetics are sufficiently fast to rapidly grow the γ' precipitates – both effects result in decreasing influence of γ' on the yield strength and a return to values similar to those predicted by the model. The final model will include the evolution of the γ' distribution and its effect on the athermal resistance to dislocation glide as well as the increase of the local dislocation climb stress for dislocation climb.

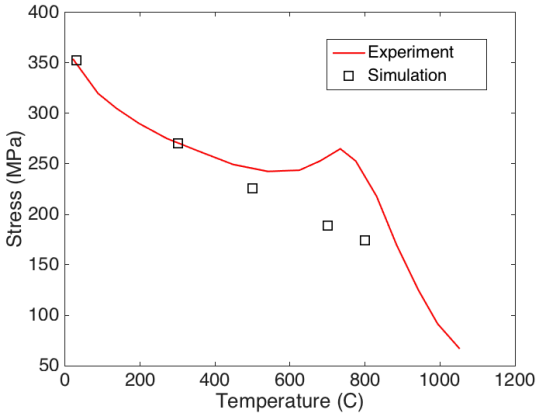

Figure 7. Yield strength with temperature.

Table 1. Experimentally calibrated parameters for the glide model

C11 (GPa)	C12 (GPa)	C44 (GPa)	G (GPa)	p	q	Activation entropy (J)	Thermal resistance (MPa)	Barrier factor	Self harden factor	Latent harden factor	Multiplication factor
220	104	70	70	0.3	1.4	8×10^{-7}	125	1.2	1.0	0.2	0.015

For the climb model, the diffusivity coefficient plays an important role in determining the creep strain. The climb velocity is given as:

$$v_c^{\alpha} = -\frac{2\pi D}{b\log(r_{\rho}/r_c)}\left(\exp(\frac{\tau V}{RT})-1\right)$$

The D is called self-diffusion coefficient and it is given as

$$D = D_0 \exp(-E_{act}/kT)$$

where E_{act} is known as activation energy for vacancy self-diffusion, is the sum of the vacancy formation and migration energies. For pure nickel, the experimental calibrated coefficients from Maier et.al [6] are D_0 = 1.33 cm^2/s and E_{act} = 2.91ev. We used the same E_{act} = 2.91ev but varied D_0 for different temperatures. The calibrated D_0 is listed in Table 2.

In our model, the evolution of vacancy concentration is given as

$$\dot{c} = -\nabla j + \sum_{\alpha} \dot{\gamma}_{c\,\mathrm{lim}\,b}^{\alpha}$$

where the first term is the contribution from the vacancy flux j in the bulk with grain boundaries and other sources or sinks. In the current model, the equation is approximated as

$$\dot{c} = \frac{k}{c_0} \sum_{\alpha} \dot{\gamma}_{c\,\mathrm{lim}\,b}^{\alpha}$$

where k is a constant and c_0 is the equilibrium vacancy concentration without applied stress. The k should decrease with the increase of the temperature because the vacancy generation and mobility becomes larger at higher temperature. The calibrated k for different temperature is listed in Table 2.

Table 2. Experimentally calibrated parameters for the climb model

	750°C	900°C	950°C
D_0 (cm^2/s)	0.033	0.006	0.019
k	20	2	0.2

The comparison of experiment and simulation for the creep strain-time at 750°C 138MPa, 900°C 26MPa, 950°C

24 MPa and 28.6 MPa is shown in Figure 8, 9 and 10, respectively. A reasonable agreement has been shown from those figures. Again, in Fig. 8 the difference between the simulation and the experimental data can be attributed to the formation of γ' and its growth at this test temperature.

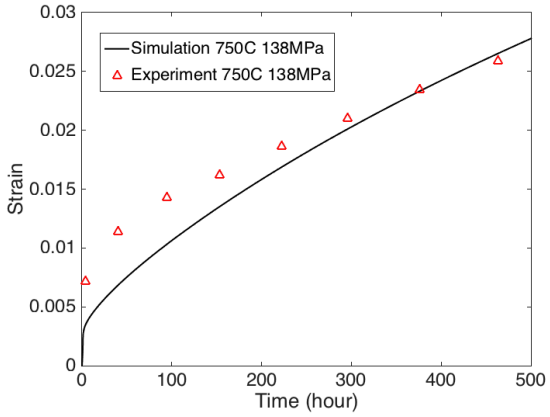

Figure 8. Comparison of creep strain response between simulation and experiment at 750°C and 138 MPa.

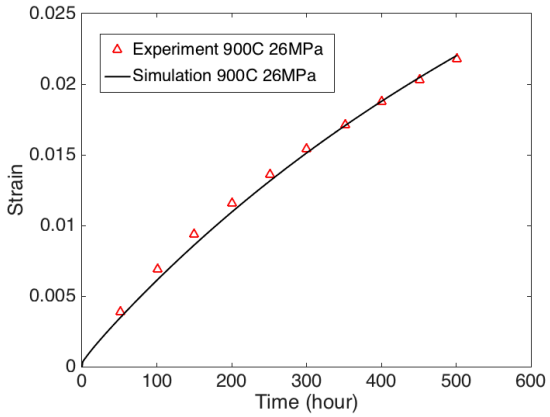

Figure 9. Comparison of creep strain response between simulation and experiment at 900°C and 26 MPa.

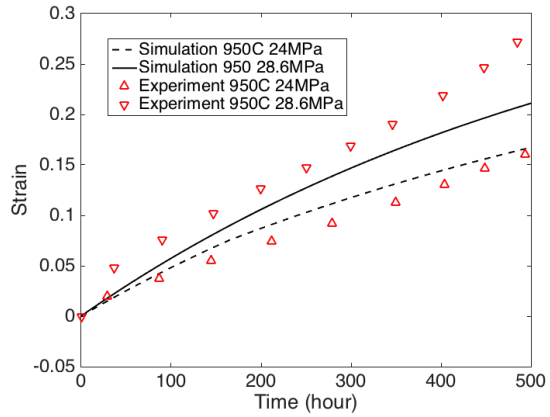

Figure 10. Comparison of creep strain response between simulation and experiment at 950°C and 24 MPa and 28.6 MPa.

The incorporation of the simulated microstructure has not been completed, as was planned but is expected to be completed by the end of the calendar year (i.e. by the end of the 1st quarter of FY18). Additionally, the dislocation/γ' interaction portion of the model has not been completed as planned in the FY17 FWP but is expected to also be completed by the end of the calendar year using FY17 carryover funds.

References:

[1] Croeber M and Jackson M, DREAM.3D: a digital representation environment for the analysis of microstructure in 3D. Integr. Matter. Manuf. Innov: **3** 5-19, 2014

[2] Chris H. Rycroft, Voro++: A three-dimensional Voronoi cell library in C++, Chaos **19**, 041111, 2009.

[3] CUBIT, Geometry and Mesh Generation Toolkit, https://cubit.sandia.gov

[4] Wright, J.K., Carroll, L.J. and Wright R.N. Creep and Creep-Fatigue of Alloy 617 Weldments, INL/EXT-14-32966, 2014

[5] Special Metals, http://www.specialmetals.com/assets/smc/documents/alloys/inconel/inconel-alloy-617.pdf

[6] K.Maiker, H.Mehrer, E.Lessmann and W.Schule, Self-Diffusion in Nickel at Low Temperatures, Physica Status Solidi (b), 78, 689 (1976)

Milestone H, "Calibration of Secondary creep"
The secondary creep rate data obtained from existing creep data on Alloy 617 from the NGNP program will be used to assess the accuracy of the model and then calibrate the model. Work on this task can only start after the dislocation/γ' interaction has been incorporated into the model which is now planned to be completed by the end of the calendar year. The completion date for this task will be moved to the end of February 2018.

Milestone I, "Stress Drop Tests"
Table 3 shows the aging matrix for the stress drop tests. Aging of all material for stress drop tests was completed in the 4th quarter of FY17. Samples have been fabricated from Plate SD-1 as well as an as-welded plate. Plate SD-2, aged for 8000 hrs at 750ºC, will be fabricated into creep samples for stress drop tests at temperatures of 700, 750 and 800ºC, early in FY18.

Two stress drop tests – one at 750ºC and one at 700ºC – on SD-1 material were started by summer intern Douglas S. Smith, Colorado School of Mines during the 4th quarter of FY17. Unfortunately, the tests are taking longer than anticipated and neither had finished by the time his internship was over. The test were still running at the end of the 4th quarter and are expected to finish in November. Seven tests remain to be completed. Additional creep frames will be utilized for the stress drop tests as they become available to accelerate testing and completion of the stress drop test matrix.

Table 3. Base Metal Aging Information for Stress Drop Tests

Sample ID	Aging Temperature	Target Aging Time, hours	Insertion Date	Expected Removal date	Status
SD-1	750	4000	9/1/2016	2/15/2017	Complete
SD-2	750	8000	9/1/2016	7/31/2017	Complete

Milestone J, "Characterization of creep failure mechanisms"
As of the end of the third quarter, nine creep tests have been completed, see Table 4. They have been mounted and polished. Characterization of these samples using optical metallography and SEM, including orientation imaging microscopy (OIM), is in the initial stages and is not complete at this time. This will require this task to be carried over to FY18 and the planned completion date for this task be moved to the beginning of February. This carryover workscope will be performed with the carryover funds from FY17.

Other highlights

Short Term Creep Tests

One short term creep test finished during the 4th quarter, 740-AWM-01 at 750°C and 305 MPa. This sample consisted of all weld metal and Figure 11 shows the creep behavior of two cross weld samples and one all-weld metal sample. Two additional all-weld metal creep tests –one at 700ºC and one at 800ºC – are planned.

Table 4. Short term creep testing parameters for modeling development

Specimen ID	Test temperature, °C	Test type	Initial Stress, MPa	Orientation	Expected rupture life, hrs	Start date	Finish date	Rupture life, Hrs
740-Q1-01	700	Rupt	413	CW*	200	8/24/2016	9/21/2016	639
740-Q1-08	700	Rupt	413	CW	500	11/28/2016	12/27/2016	670.8
740-Q1-06	700	Rupt	395	CW	1000	01/09/2017	02/16/2017	879.3
	700	Rupt	344	CW	1000			
740-Q1-03	750	Rupt	350	CW	200	9/29/2016	10/07/2016	184
740-Q2-01	750	Rupt	350	CW	200	05/03/2017	05/10/2017	162
740-Q1-05	750	Rupt	305	CW	500	10/18/2016	11/06/2016	450
740-Q2-02	750	Rupt	305	CW	500	05/03/2017	05/18/2017	355
740-Q1-10	750	Rupt	230	CW	1000	03/10/2017	05/24/2017	1749
740-Q1-04	800	Rupt	240	CW	200	10/10/2016	10/15/2016	123.6
740-Q1-02	800	Rupt	200	CW	500	11/08/2016	11/22/2016	326.8
	800	Rupt	138	CW	1000			
	700	Rupt	400	AWM**	500			
740-AWM-01	750	Rupt	305	AWM	500	06/19/2017	8/12/2017	1272.5
	800	Rupt	144	AWM	500			

* CW = Cross weld

** AWM = All Weld Metal

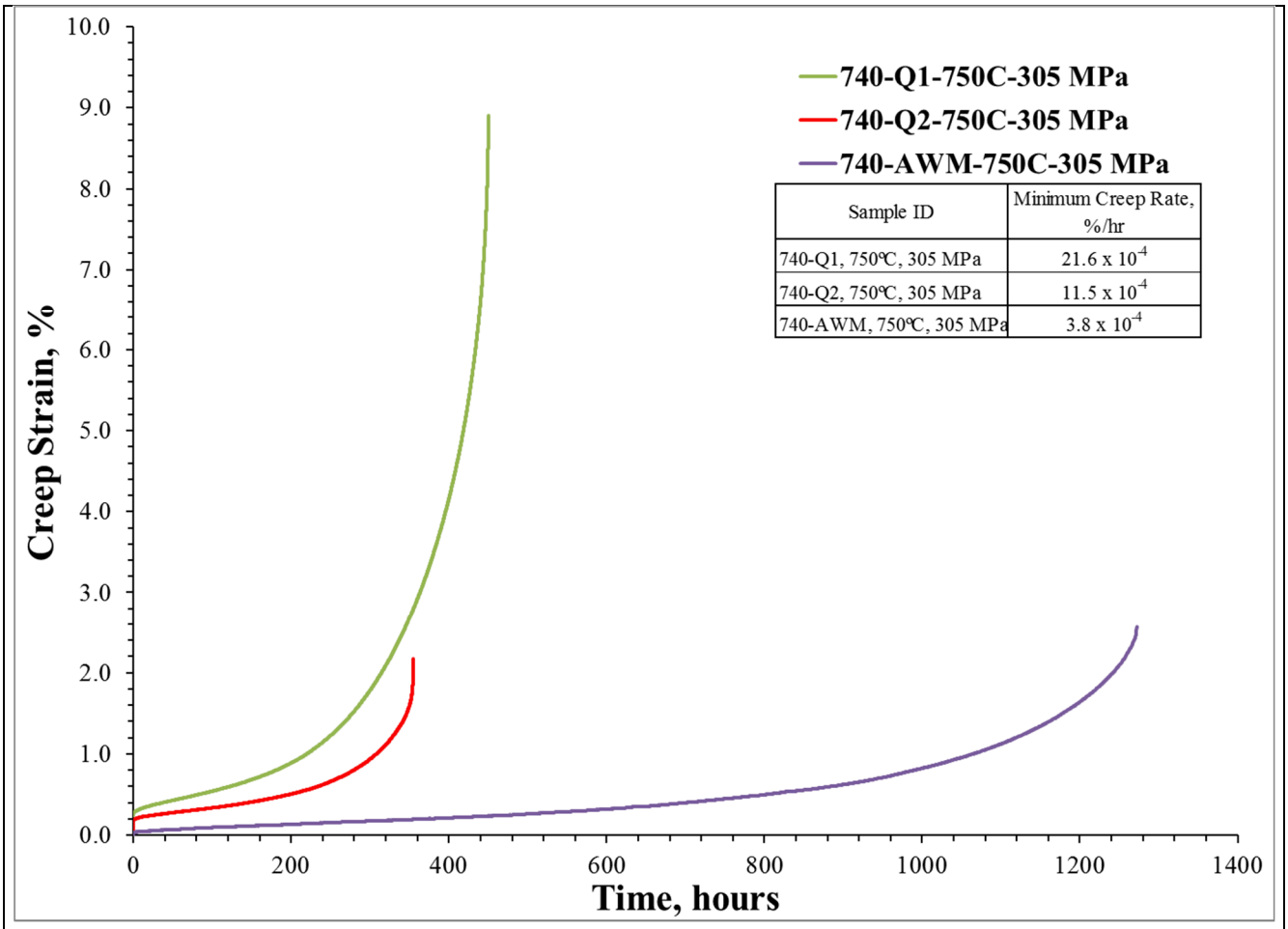

Sample ID	Minimum Creep Rate, %/hr
740-Q1, 750ºC, 305 MPa	21.6×10^{-4}
740-Q2, 750ºC, 305 MPa	11.5×10^{-4}
740-AWM, 750ºC, 305 MPa	3.8×10^{-4}

Figure 11. Plots of creep behavior for cross weld samples and all-weld metal creep samples under the same conditions.

Long Term Creep Tests

Both long term, cross-weld creep tests for verification of the final creep simulation finished during the 4th quarter of FY17. Figure 12 shows the creep behavior of the two samples. Both tests were expected to run on the order of 9700 hours. However, the sample tested at 800ºC failed during the second quarter of FY17 after only 4592 hrs while the other long term test at 750°C and 141 MPa has exceeded 10,200 hrs and is still running. The creep ductility for the failed sample was low, <10%, which has been typical of the shorter term cross-weld creep tests. Upon failure of the sample in the 750ºC test, metallography will be performed on both samples to study the failure mode.

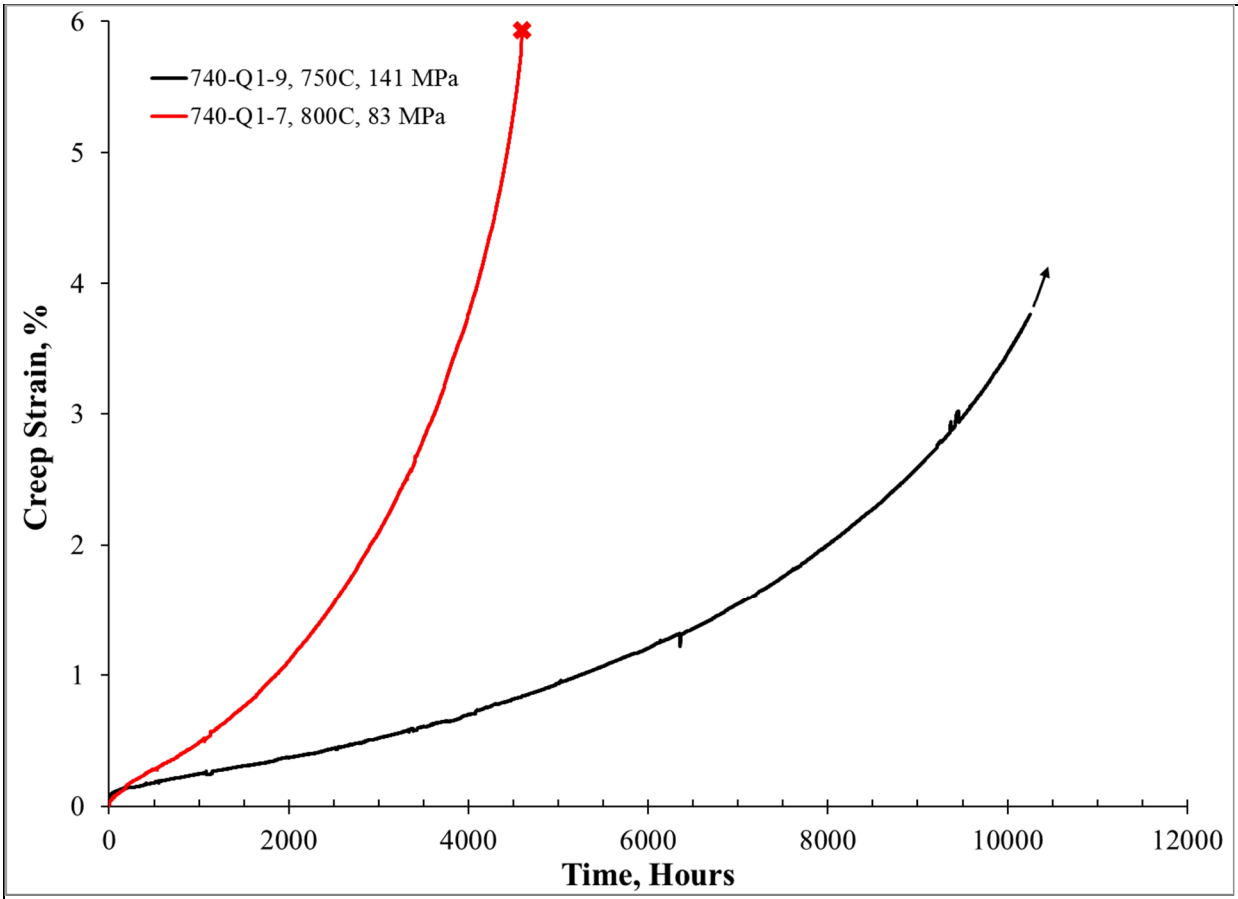

Figure 12. Creep behavior of two long term creep tests. Expected creep life for both tests was on the order of 9700 hours.

γ' Aging Study

Aging of welds at 700, 750 and 800°C continues. TEM samples extracted from the HAZ by focused ion beam (FIB) methods and observed in the TEM at the Center for Advanced Energy Studies (CAES) resulted in relatively poor quality TEM micrographs of the γ' particle, Figure 13. Therefore, TEM samples of the base and weld metal were prepared by sectioning and grinding. Then, 3 mm discs were punched from the blanks and electropolished. Figure 14 shows that the particles in the electropolished sample are much more defined than in the FIB-prepared sample, shown in Figure 13. Therefore, it appears that analysis of the γ' particle distributions will have to be carried out on electropolished samples. This will be suitable for base and weld metal. However, difficulties may be encountered when the γ' distribution in the HAZ will be studied. The HAZ is approximately 1 mm wide and obtaining electron-transparent area in this specific region will require careful preparation. Also, the importance of the γ' distribution in the HAZ may not be significant since creep failures have, to this point, all occurred in the middle of the weld, relatively far from the HAZ.

Also, a backlog of aged samples need to analyzed for the γ' size and spatial distributions. Performing dark field imaging of the particles in the TEM, as shown in Figure 14, is rather time-consuming. Alternatively, imaging the particles the high angle, annular dark field (HAADF) detector, which highlights very small differences in

composition, shows promising in accelerating the analysis of samples, Figure 15. (The location of the images in Figs. 14 and 15 are different and the particles in Fig. 15 show cuboidal particles that are relatively tightly spaced. The particles in Fig. 14, however, show less cuboidal tendencies and are more widely spaced, indicating the γ' distribution and γ' morphological characteristics vary with location in the weld metal, most likely due the compositional segregation that occurs during solidification of the weld metal.

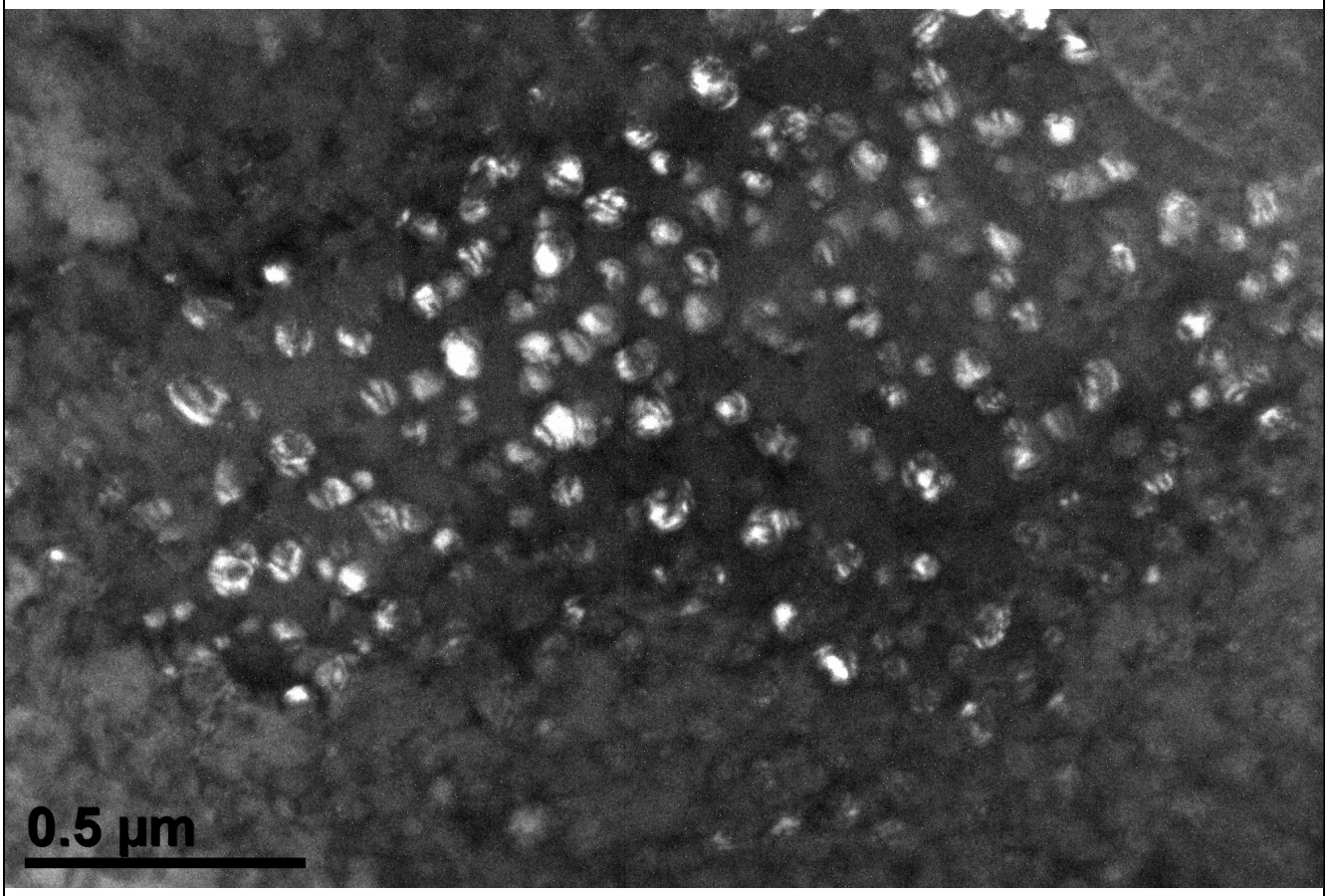

Figure 13. Dark field TEM image showing γ' particles in the HAZ of welds aged for 3000 hrs. Sample was produced by FIB methods.

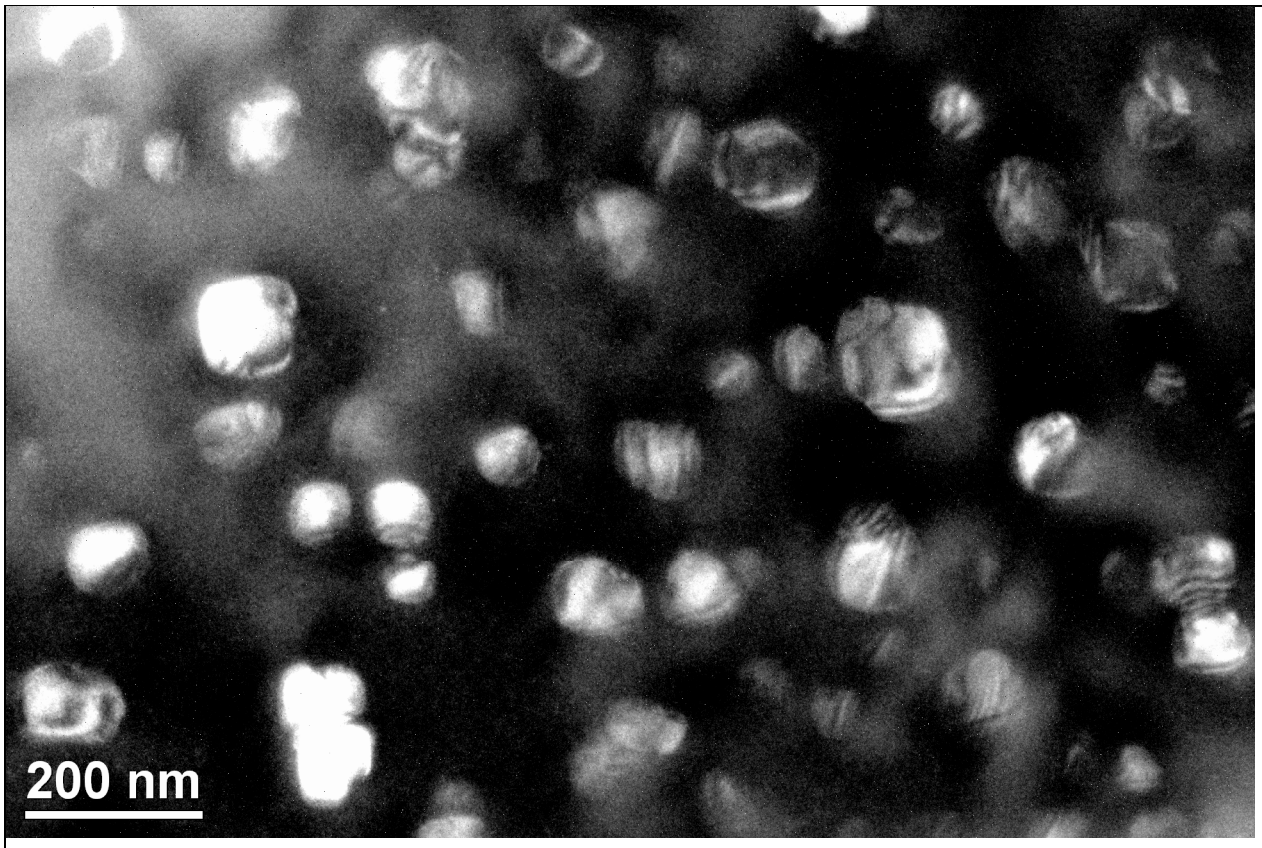

Figure 14. Dark field image of γ' particles in weld metal, aged for 3000hrs at 750C. The sample was prepared by electropolishing.

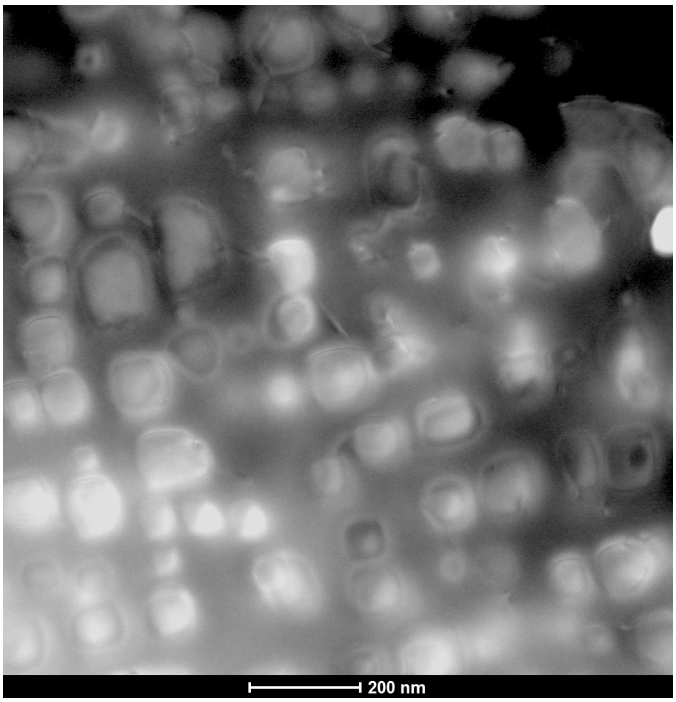

Figure 15. STEM image using the HAADF camera to image the γ' particles.

ISSUES

Both the modeling effort and the experimental data acquisition and characterization have fallen somewhat behind schedule. However, the effort for FY17 finished about $36k under budget and should allow the project to get back on schedule.

Report Prepared By	Date
Thomas M. Lillo	10/24/2017